RJC

RASĀYAN *J. Chem.*
Vol. 18 | No. 3 |1305-1315| July-September | 2025
ISSN: 0974-1496 | e-ISSN: 0976-0083 | CODEN: RJCABP
http://www.rasayanjournal.com
http://www.rasayanjournal.co.in

MAGNETIC AND PHOTOCATALYTIC PROPERTIES OF SAMARIUM DOPED STRONTIUM HEXAFERRITES SYNTHESIZED BY AUTO-COMBUSTION METHOD

A. Thippeswamy[1], Prabhakar Chavan[2] and G. Krishnamurthy[3,✉]

[1]Department of PG Studies in Industrial Chemistry, Government Arts and Science College, Karwar -581301, Karnataka, India- 581301

[2]Department of PG Studies and Research in Chemistry, Sahyadri Science College, Constituent College of Kuvempu University, Shivamogga, Karnataka, India-577203

[3]Department of PG Studies in Industrial Chemistry and Chemistry, Sahyadri Science College, Constituent College of Kuvempu University, Shivamogga-577203

✉Corresponding author: gkmnaiksahyadri@gmail.com

ABSTRACT

In this study, samarium-doped strontium hexaferrites $SrFe_{12-x}Sm_xO_{19}$ (x=0, 0.01, 0.05, and 0.09) SmSrHF's were synthesised by the auto-combustion method, assisted by urea as a fuel. The microstructural properties of SmSrHF's were characterized by XRD, FTIR, UV-Visible, VSM, SEM, and EDAX. The XRD spectral data indicate a crystalline nature with a crystal size ranging from 30-40 nm, which matches with standard JCPDS card number 24-1207. The M-H curve showed the saturation magnetization (Ms) in the range 36.05-40.31 emu/g and remanence (Mr) 20.13-22.61 emu/g, which increases as the substitution of samarium ions increases. VSM investigated the hard magnetisation and permanent magnet. The energy band gap determined was around 2.5 eV. The photodegradation ability of synthesized SmSrHFs on different dyes was examined in the presence of sunlight. 4-nitroaniline dye undergoes effective photocatalytic degradation when compared to other tested dyes. SmSrHF acts as a good photocatalyst with easy recyclization when compared to metal oxide NPs.

Keywords: Auto-Combustion, EDAX, Magnetization, Photodegradation, Samarium, Strontium Hexaferrites.

RASĀYAN *J. Chem.*, Vol. 18, No. 3, 2025

INTRODUCTION

In recent decades, there has been a drastic increase in human population, which has led to an increase in the use of essential commodities like semiconductor materials, cosmetics, chemicals for agriculture, pharmaceutical products, food preservatives etc., The excessive use of consumables leads to the discharge of many harmful chemicals, which adversely effect on environment and cause ill effects on aquatic life, which in turn affect the human health system. Upcoming research should focus on solving such problems to the maximum extent. In this context, a few novel nano-particles (NPs) have been synthesised by different research groups across the world, and their applicability in solving some of the above ill effects has been studied. A few newly synthesized nanoparticles exhibit semiconductor behaviour in the presence of UV light or sunlight due to their favourable electronic structure for absorbing or emitting the light, and thus serve as a catalyst for a variety of applications in semiconductor industries.[1] In addition, researchers focused to determine the breakdown of larger sized toxic organic molecules into simple size by photocatalytic reactions in the presence of synthesised nanoparticles thereby minimising the adverse effects on the public health and environment.[2] Nanomaterials also play an important role in the development of multiple technologies such as sensors, biomedical science, surface science etc., and industries like electronic, semiconductor, optics, magnetism, electrochemistry, aerospace, agriculture, biotechnology, national defence, information technology, medicine and transportation.[3] Doping is a technique where a metal ion of specific properties is inserted into the lattice site of a known nanomaterial to enhance or impart required properties. Doping is done by using a suitable transition or rare earth metal ions having variable oxidation states. Structural modification by doping of different metal ions into ferrites and their application is well studied.[4] Many doped nanoparticles show a significant role and have important applications in biological, semiconducting, and photo-optical properties.[5] Doping a very small

http://doi.org/10.31788/RJC.2025.1839272

amount of rare-earth metal ions into ferrites alters their structural, morphological, magnetic, and electrical properties. Literature of the recent decade indicated that some semiconductor nanomaterials (ZnO and TiO_2) are extensively applied as dopants due to their biological, chemical inertness, easy availability, and lower cost.[6] In addition, several samarium (Sm) doped MnO_xTiO_2 catalysts were used for the selective catalytic reduction of NO_x with NH_3. The Sm in the catalyst can enhance the surface area and thus increase the surface-active sites, which result in NO_x conversion.[7] In photodegradation application where a bulkier toxic organic molecule is broken into smaller molecules having lower toxicity in the presence catalyst and sunlight, Sumadevi *et.al*., have synthesised Poly(vinyl pyrrolidone) capped and uncapped Co: ZnS nanoparticles and studied their photodegradation properties.[8] Research from our laboratory focuses on structural, optical, and photocatalytic properties of synthesised novel nanoparticles.[2,9,11] In continuation, in the present research, the samarium substitution in strontium hexaferrites has been prepared by a simple and low-cost auto-combustion method using urea as a fuel; their structural variation and photocatalytic properties have been studied.

EXPERIMENTAL

Materials and Methods

The precursors and organic fuels used were of analytical grade, Ferric nitrate nano-hydrates, $Fe(NO_3)_3.9H_2O$, Samarium nitrate hexahydrate, $Sm(NO_3)_3.6H_2O$, strontium nitrate, $Sr(NO_3)_2$, and urea (CH_4N_2O) and distilled water. The synthesized SmSrHF's nanoparticles were characterized using powder X-ray diffraction, Philips diffractometer (Bruker, d8 Advance, Germany) using Cu-Kα radiations (λ=1.5406Å). The FTIR spectra of all samples were recorded on a Shimadzu spectrometer (Spectrum 2 USA). Microstructure was observed by scanning electron microscopy, JEOl/EO/JSM-639, and the energy dispersive X-ray spectrum was recorded using (CarlZeiss, EVOLS15). Saturated magnetism (Ms), remanence Magnetism (Mr), and Hc of all SmSrHF's were determined at 300K using VSM (Vibrating Sample Magnetometer (20130523-01)), which was employed to characterize the magnetic properties. Thermo gravimetric analysis (NETZSCH, STA 2000) for the analysis of thermal behaviours of the prepared samples. Systronics UV-Visible spectrometer 119 was employed for Dye degradation studies.

General Procedure

Samarium-doped Strontium hexaferrites (SmSrHF) nanostructured materials were prepared through the auto-combustion method. The metal precursors used were, $Fe(NO_3)_3.9H_2O$, $Sm(NO_3)_3.6H_2O$, $Sr(NO_3)_2$ and (CH_4N_2O) which were purchased from Sigma Aldrich and Sd fine chemicals and were used in the stoichiometric ratios of Fe^{3+}, Sm^{3+}, Sr^{2+} ions in aqueous solution in a cylindrical petri dish carrying the solution of redox mixture and then placed into a furnace to attain the temperature to 500℃, at which N_2O and CO_2 gases were released and also a large amount of heat. The whole reaction was carried out in four minutes with a smouldering process.[10] The sintered powders were ground in a mortar with a pestle. The loose powder NPs were heated at 1100 ℃ and maintained for 3h, and then slowly cooled to room temperature. Synthesized NPs were stored in an airtight vial for further investigation.

Photocatalytic activity

Water soluble dyes like Erichome black-T **(**EBT), Methyl blue (MB), Methyl orange (MO), and 4-nitroaniline (4-NA) were tested for degradation in the presence of sunlight and SmSrHF as a catalyst in different concentrations in percentage and at different time intervals. In the catalytic reaction, 0.0001 g of SmSrHF sample was dispersed in 30 mL of double-distilled water under sonication, then poured into the solution of dye. Initially, the solution was stirred in the dark at room temperature for 1 h, and the UV-visible absorption spectra of it were recorded to compare the spectra before and after degradation. After that, the solution was kept in the sunlight with occasional mechanical stirring. At every 30-minute interval, 1 mL of the reaction mixture was withdrawn from the solution kept under sunlight to record UV-visible spectra, which helps to determine the photodegradation of dyes.[11]

RESULTS AND DISCUSSION

X-Ray Diffraction

Determination of the crystalline structure of SmSrHF's in different concentrations using X-ray diffraction analysis is shown in Fig.-1. The peaks with h, k, l values of planes (110), (114), (200), (205), (304), and

(203) compared with the JCPDS card number 24-1207, which matches the hexagonal phase. $\frac{1}{d^2\ hkl} = \frac{4}{3}\left(\frac{h^2+hk+l^2}{a^2}\right) + \frac{l^2}{c^2}$ Where h, k, l are the Miller indices and d_{hkl} are the crystal planes, a and c are the lattice parameters. XRD studies showed that the lattice parameter increased slightly from 0.51068 to 0.57286 cm^{-1}, the unit cell volume of the hexagonal system is determined by the relation V cell = 0.866 a^2c, where a and c are the lattice parameters sustained for the hexagonal system.[12]

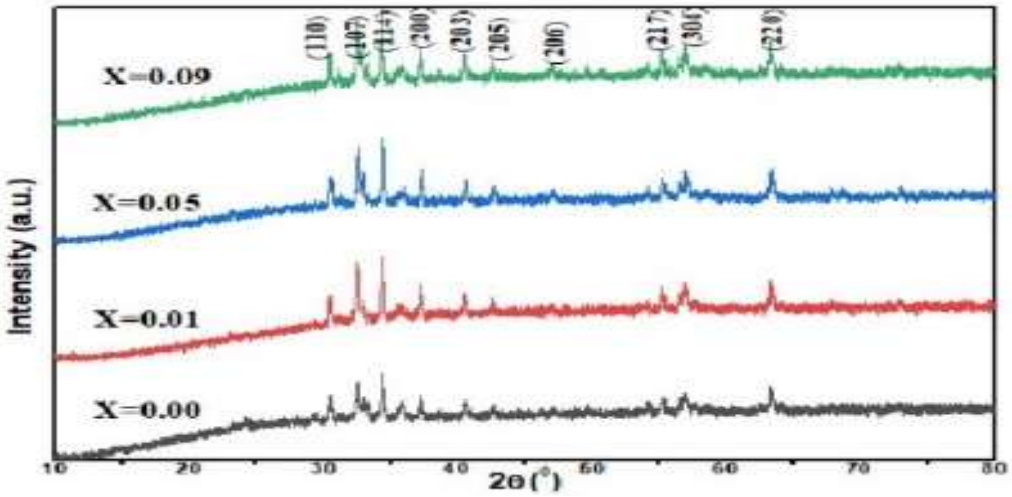

Fig.-1: XRD Pattern of $SrFe_{12-x}Sm_xO_{19}$ (x=0, 0.01, 0.05 and 0.09)

From the XRD profile, an average size of nanoferrite crystallites was found by the Debye-Scherrer equation (d) and is calculated by Scherrer's formula. D = Kλ/βcosθ, where K 0.89 is a constant of Scherrer's value for the hexagonal system, λ = 0.15406 nm is the wavelength of the incident X-rays, θ is the Bragg diffraction angle, and β is the FWHM of the diffraction peak. The average value of crystallite size obtained was in the range 30-40 nm, and their values are tabulated in Table-1. Hypothetical X-ray thickness (dx) of each sample was determined using the formula Dx = ZM/NV, where Z = 2 is the number of particles per unit cell, M is the atomic weight, N is Avogadro's number, and V is the unit cell volume.

Table-1: Crystallite Size (D), Lattice Constant (a & c), Cell Volume (V), and X-Ray Density (qx-ray) of SmSrHF's

Composition	Crystallite size (D) /nm	Lattice constant (a)/Å	Lattice constant (c)/Å	(c)/(a) Å	Cell volume (V)/$Å^3$	X-ray density (qx-ray)/g cm^{-3}
$SrFe_{12}O_{19}$	31.02	5.8794	22.358	3.9133	691.38	0.5106
$SrSm_{0.01}Fe_{11.99}O_{19}$	30.63	5.8814	23.0180	3.9161	691.36	0.5806
$SrSm_{0.05}Fe_{11.95}O_{19}$	30.39	5.8814	23.0180	3.9161	691.30	0.5760
$SrSm_{0.09}Fe_{11.91}O_{19}$	30.29	5.8814	23.0180	3.9161	691.35	0.5728

The cell volume of the SrHF's patterns was set in various boundaries, such as a, c, and Vcell are tabulated in Table-1. X-ray thickness is in the range 0.5106 - 0.5728 cm^{-1}. The decrease in thickness is more due to the doping of larger molecular weight (104.14 amu) and ion volume (0.1034 nm) of the Sm^{3+} Ion. When compared to the smaller molecular weight (87.62 amu) with larger ion radius (0.112 nm) of strontium ions.

Fourier Transform Infrared Measurements

The FTIR analysis for SmSrHF's nanocomposites synthesised in different concentrations is shown in Fig.- 2. Two bands at 502 and 587 cm-1 are observed for the hexagonal lattice and are the direct result of metal-oxygen stretching vibrations.[13,14]

On doping Sm^{3+}, the position of the peak slightly shifts to the lower wave number, indicating replacement of Sr^{2+} by Sm^{3+} without changing the crystal structure of the composition. Further, the absence of the band in the region 300- 4000 cm^{-1} showed the non-existence of the –OH group in the reaction product.[15]

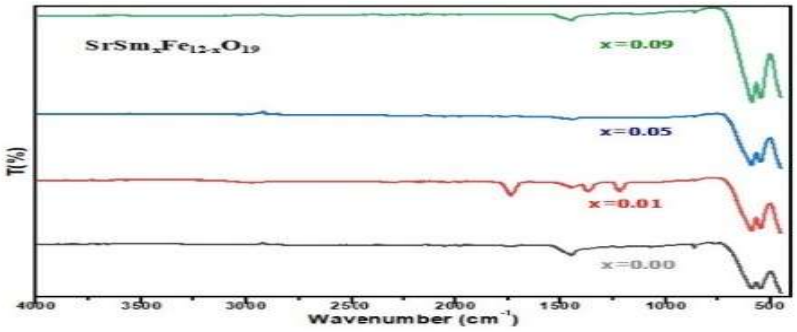

Fig.-2: FTIR Spectra of Sintered Powder of $SrFe_{12-x}Sm_xO_{19}$ (x=0, 0.01, 0.05 and 0.09) Nanoferrites

SEM and EDAX Analysis

The morphology and particles size of $SrFe_{12-x}Sm_xO_{19}$ (x=0, 0.01, 0.05 and 0.09) depicted Fig.-3(a)-(d). The SEM image confers the grains' morphology and clearly shows hexagonal-like contour platelets, a rough, irregular, clustered surface, and a crystalline nature of M-type SmSrHF's nanoferrites. The elemental mapping by EDX is shown in Fig.-4(a-c) for SmSrHF's (x < 0.00 <0.09). The presence of strontium, iron, samarium, and oxygen is observed. The results of EDX measurements show that the appearance of their corresponding peaks without any other characteristic peaks suggests that the prepared samples are not contaminated during the synthesis process.

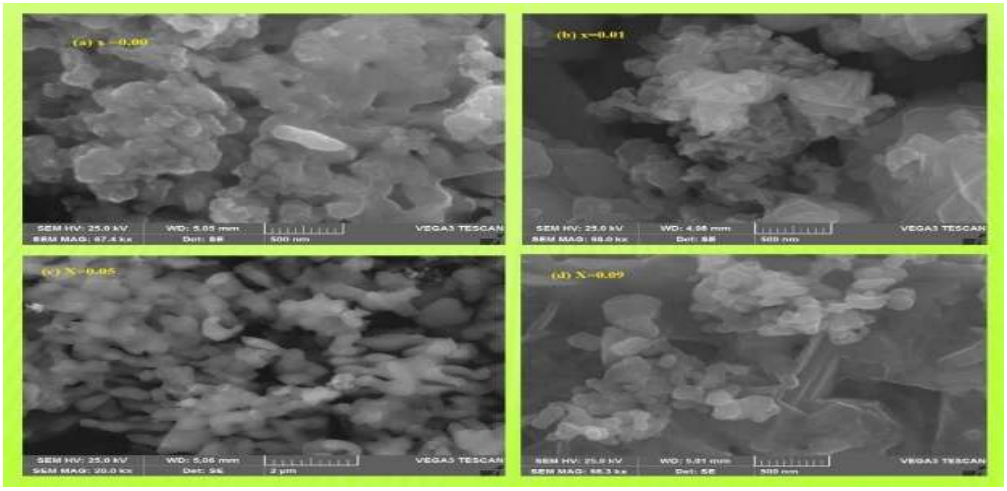

Fig.-3(a-d): SEM Micrographs of M-type Hexaferrites $SrFe_{12-x}Sm_xO_{19}$ for all Compositions
(a) x=0, (b) x=0.01, (c) x=0.05 and (d) x=0.09

Magnetic Properties

The magnetization curve as a function of applied magnetic field of 8Oe with a maximum field of 70 Oe at room temperature. Different compositions of samples were analysed by using a vibrating sample Magnetometer (VSM). Figure-5 shows MH-loops for M-type hexagonal ferrites $SrFe_{12-x}Sm_xO_{19}$ (x=0.0, 0.01, 0.05, and 0.09) than a typical ferromagnetic. The magnetic properties, such as retentivity (Mr), coercivity (Hc), Saturation magnetization (Ms), and Squareness ratio (Mr/Ms), are extracted from hysteresis curves and presented as a function of the Sm doping content[16] in Fig.-5. The electronic configuration of substituted cations (or doped material) affects the magnetic properties of substituted hexagonal ferrites. The electronegativity of substituted samarium (Sm^{3+}) is 1.17. Every Fe^{3+} ion in the skeleton has five unpaired electrons, and in addition, hexagonal ferrites have five different sub-lattices that are occupied by a total of 12 $Fe^{3+,}$ three octahedral (12k, 2a, $4f^2$), one tetrahedral ($4f^2$), and one is trigonal bipyramidal (2b). Of these 12 Fe^{3+} ions, four have the spin in the downward direction that is at $4f^2$ (2 Fe^{3+}) and $4f^2$ ($2Fe^{3+}$) while other 8 Fe^{3+} ions have the spin in upward direction that is at 12k (6 Fe^{3+}), 2a (1 Fe^{3+}) and 2b (1 Fe^{3+}). The four downward spins and four upward spins cancel each other, and the remaining 4 Fe3+ ions, which have an upward direction, contribute to the magnetic moment.[17]

The values of retentivity (Mr) and saturation magnetization (Ms) are reduced due to the addition of the concentration of Sm^{3+} ions. The magnetic parameters were calculated using the following relationship:

$$\eta\beta = \frac{\text{M X Ms}}{5585}$$

$$s = \frac{\text{Mr}}{Ms}$$

$$K = \frac{Hc\ X\ Ms}{2a0.64}$$

Where, ηβ Is the magnetic movement/ formula unit (μb), remanence magnetization, Ms– saturation magnetization (emu/g), M – molecular weight in g, 5585-magnetic factor, K-magnetic anisotropic constant, and Hc- coercivity.

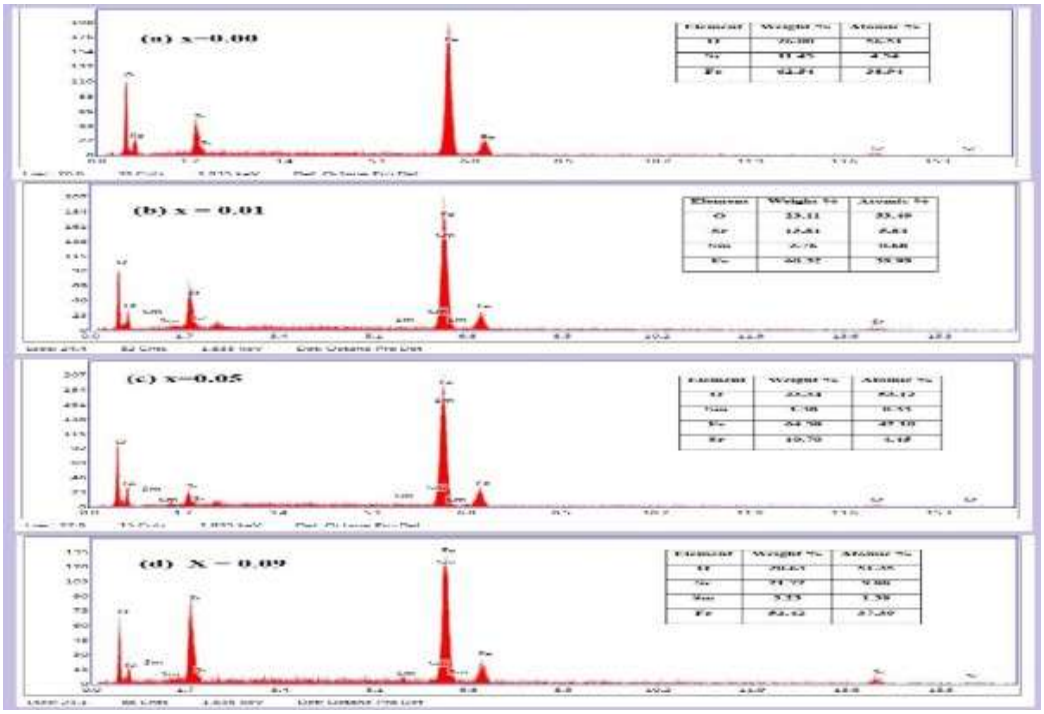

Fig.-4(a-d): Elemental Mapping and EDX Spectrum of $SrFe_{12-x}Sm_xO_{19}$ Nanoparticles (a) x=0.00, (b) x=0.01, (c) x=0.05 and d) x=0.09

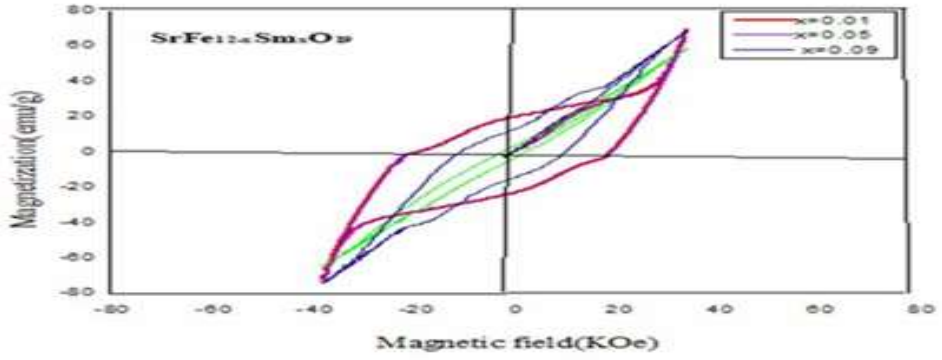

Fig.-5: Hysteresis Curves of $SrFe_{12-x}Sm_xO_{19}$ (x=0.0, 0.01, 0.05, and 0.09) Nanoferrites

Magnetization is enhanced with A-site substitution. The Sm^{3+} ions have a smaller magnetic moment than Fe^{3+} ions. At B locale, the number of Fe^{3+} ions increased, so the magnetization of the B sublattices increased.[18] So the magnetization was enhanced in the Sm^{3+} substituted samples. Results show that as the doping of samarium increases, consistently the saturation magnetization and remanence increase, and that decreases. The increase of the Ms value when x=0.09. The presence of Fe_2O_3 contributes to maintaining

electrical neutrality in the strontium hexaferrite. However, the increase of hyperfine fields in the 12K and 2b sites due to the superexchange interaction in Fe^{3+}- O - Fe^{3+} leads to a higher magnetization in the lattice.[19] Also effects the relative ionic radii Sm^{3+} and (host) Fe^{3+}ions, which are (0.96Å) and (0.64Å) causes decrease of Ms Value. The magneto-crystalline anisotropy is responsible for the decrease due to the presence of the Fe^{3+} ion site, which is usually present in the rare earth substituent. Hence, the coercivity 9(Hc) reduces with increasing substituent concentration, which may be because of the difference in size of the ionic radii of the host and dopant. The ionic radii of Sm^{3+} ions replaced the Fe^{3+} ions from $4f^2$ sites, and due to this, Hc decreases. Usually, in all hexagonal ferrites, one large divalent metal ion (Pb, Ba, or Sr) is mostly present, which causes a trivial interruption in the lattice because of their difference in size. In most cases, the c-axis is the favoured orientation in all hexagonal ferrites. Hence slack crystals line up themselves within the c-axis when the direction of the applied field is perpendicular, and haphazardly orient when the field direction is parallel.[20]

Table-2: Retentivity (Mr), Saturation Magnetization (Ms), Coercivity (Hc), and Magnetic Moment (μB) Hexaferrites for all Compositions of $SrFe_{12-x}Sm_xO_{19}$ (x=0.00, 0.01, 0.05, and 0.09)

Sample name	Ms(emu/g)	Mr(emu/g)	Mr/Ms	Hc(Oe)	nβ(uβ)
SF1	36.051	20.137	0.55	4873	7.80
SF2	34.536	19.398	0.56	5154	7.43
SF3	40.130	22.615	0.56	6135	8.57

UV-Visible Studies

The UV-Visible spectra of SrHF's nanoparticles displayed an excitonic peak centered around 370 nm. The fundamental property of semiconductors is the band gap, which is measured by UV-Visible spectroscopy. UV-Visible spectra of bare strontium ferrite gave a band at 320 nm, and samarium-doped Strontium ferrites at 370 nm. The band gap of pure nanoparticles was 2.5 eV. The band gap value of pure and doped NPs indicates that the synthesized nanoparticle acts as a semiconductor (0- 3 eV).[21] The Kubelka-Munk (K-M) theory was used to determine the band gap of nanoparticles. Using the following relation.

$F(R\infty) = \frac{(1-R\infty)^2}{2R\infty}$ Where h is the Planck constant (6.626 x 10^{-34} Js), C-Speed of light (2.99 x 10^8 ms^{-1}), λ is the wavelength of reflectance spectra, and R∞ is the diffuse reflectance spectra. α –Absorption coefficient, ν -Frequency of the incident light, and Eg -Band gap energy. The obtained band gap of SmSrHF's $SrFe_{12-x}Sm_xO_{19}$ (x=0, 0.01, 0.05, and 0.09) NPs, 2.5 eV, confirmed that SmSrHF's NPs are UV active material.

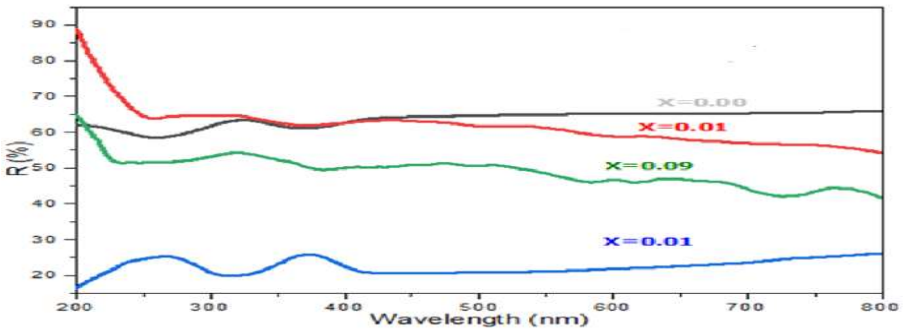

Fig.-6: The reflectance spectra of $SrFe_{12-x}Sm_xO_{19}$ (x=0, 0.01, 0.05 and 0.09)

Photocatalytic Activity

The photodegradation efficiency of synthesised $SrSm_{0.09}Fe_{11.91}O_{19}$ has been determined on Eriochrome black-T (EBT), methyl Orange (MO), methyl blue, and 4-nitroaniline(4-NA) under UV light illumination. However, 98% degradation results were obtained with $SrSm_{0.09}Fe_{11.91}O_{19}$ using 4-nitroaniline dye, and $SrSm_{0.09}Fe_{11.91}O_{19}$ was used as a catalyst. All dyes undergo degradation in different time intervals under the sunlight in the presence of the synthesized $SrSm_{0.09}Fe_{11.91}O_{19}$ nanoparticles as a catalyst. The probable mechanism of photodegradation is represented in the following Scheme-1.

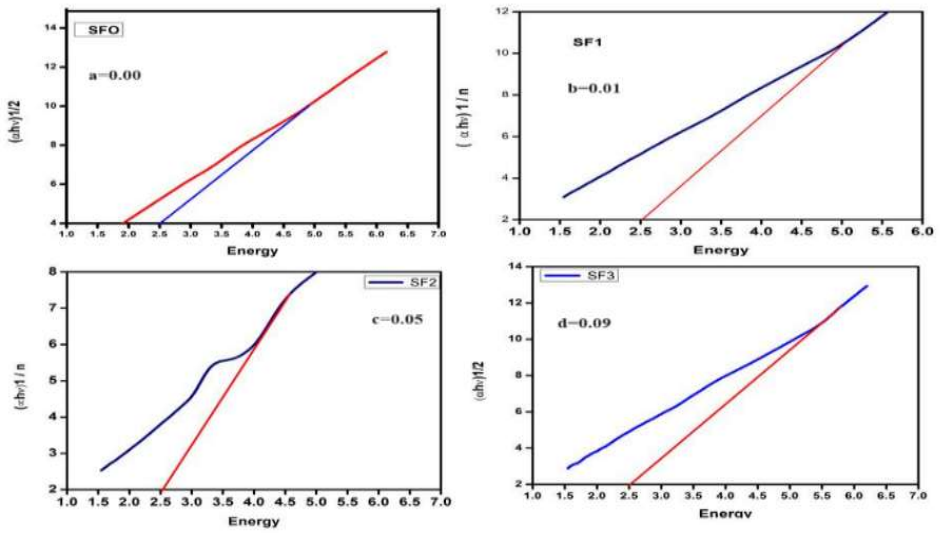

Fig.-7: UV-Vis Absorption Spectra of $SrFe_{12-x}Sm_xO_{19}$ (x=0, 0.01, 0.05 and 0.09)

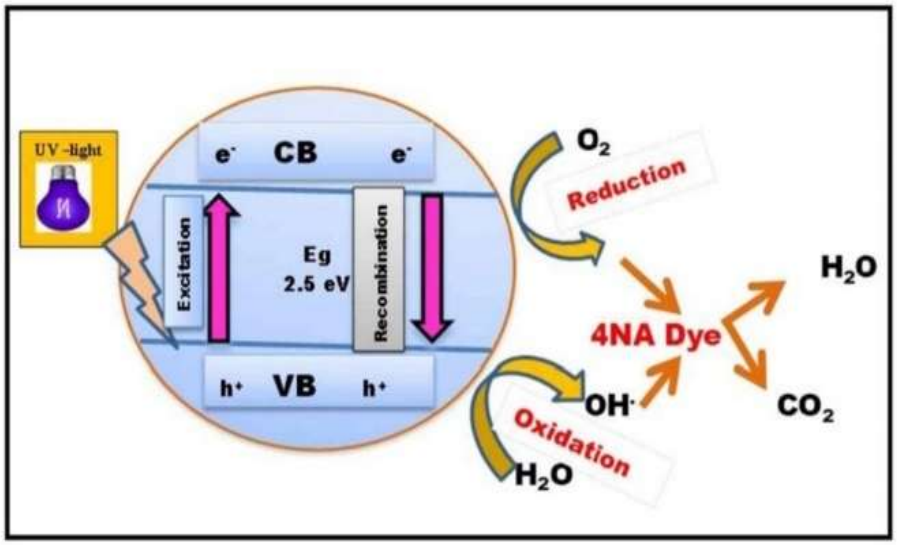

Scheme-1: Mechanism of Dye Degradation in the Presence of $SrSm_{0.09}Fe_{11.91}O_{19}$ under UV Light

$SrFe_{12-x}Sm_xO_{19} + h\nu\ (vis) \rightarrow SrFe_{12-x}Sm_xO_{19}\ (e^-CB + h^+VB)$
$SrFe_{12-x}Sm_xO_{19}\ (e^-CB) + O_2 \rightarrow O_2^{\cdot}$
$O_2^{\cdot} + h^+ \leftrightarrow HOO^{\cdot}$
$2HOO. \rightarrow H_2O_2 + O_2$
$SrFe_{12-x}Sm_xO_{19}\ (h^+VB) + H_2O \rightarrow HO^{\cdot} + H^+$
$Dye + HO^{\cdot} + O_2^{\cdot} \rightarrow CO_2 + H_2O$ (Byproduct)
$Dye + SrFe_{12-x}Sm_xO_{19}\ (h^+VB) \rightarrow$ Oxidation Product
$Dye + SrFe_{12-x}Sm_xO_{19}\ (e^-CB) \rightarrow$ Reduction Product

Among the products formed, hydroxyl radicals (•OH) are the most significant contributors in dye degradation. Scheme-1 shows a schematic illustration of dye degradation utilizing SmSrHF's under sunlight. During photo excitation, electrons in the conduction band (CB) and holes in the valence band (VB) are created. The photogenerated electrons in the CB react with molecular oxygen to produce anionic superoxide radical ($\bullet O_2$) through reduction.[22] Electrons attract to the photogenerated holes in VB by hydroxyl ions or water molecules to produce the most reactive hydroxyl radical (•OH) over oxidation.[23]

The H_2O_2 produced due to the superoxide anion radicals interacts with e/h^+ pairs. On the SmSrHF's surface, the organic molecules are attacked by these effective species, which act as strong oxidizing agents. As a result, these organic dye molecules are easily attacked by ions, leading to form by-products.[24] This is known as the redox reaction, which occurs on the photocatalyst's surface. The comparison of photodegradation studies of SmSrHF's against EBT, MO, and 4-NA is shown in Fig.-8. UV-Visible spectroscopy was used to record the decolourisation of EBT, MO, MB, and 4-NA over the surface of SmSrHF's. Initially, no change in colour of dyes was observed in UV-visible spectra. However, on irradiation with light, all dyes degrade. Among the tested dyes, 4-NA undergoes easy degradation in a shorter time when compared to other dyes.

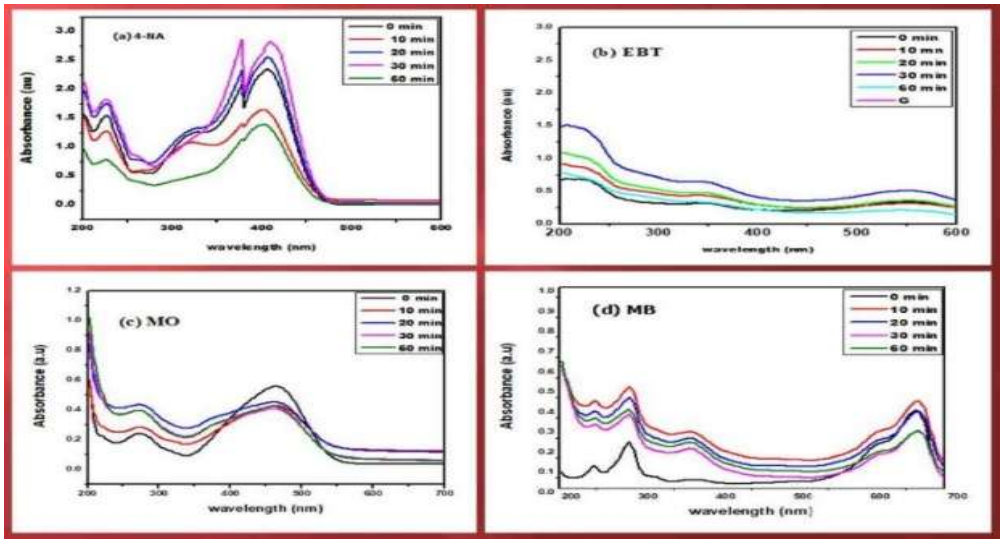

Fig.-8: Band Gap Energy of different Dyes at Different Time Intervals in the Presence of $SrSm_{0.09}Fe_{11.91}O_{19}$

Thus, only 4-NA was considered for further photodegradation studies. In continuation, the photodegradation was conducted at parameters like variable concentration of dye and different amounts of catalyst, at different pH conditions etc. The graphs showing the effect of concentration and catalyst load are represented in Fig.-8, and under different pH conditions are shown in Fig.-9.

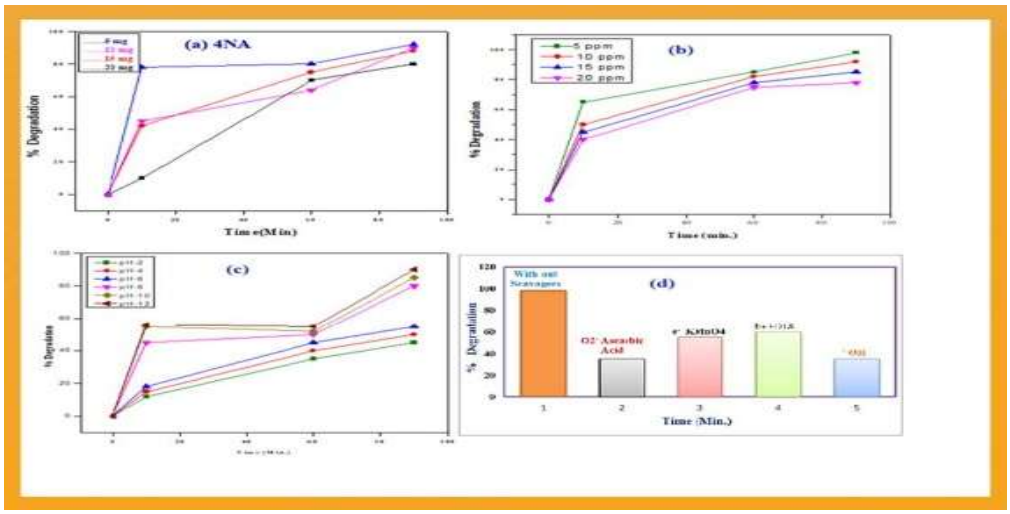

Fig.-9: Photocatalytic Activity of $SrSm_{0.09}Fe_{11.91}O_{19}$ (a) Effect of Concentration, (b) Effect of Catalyst Load, (c) Effect of pH, (d) Effect of Different Scavengers during the Degradation of 4-NA

Effect of Dye Concentration

The degradation of 4-NA in different concentrations was studied, which was required for successful photocatalytic studies. Therefore, different concentrations of dye were prepared from 5 to 20 ppm with a

catalyst amount of 20 mg per 100 mL, as illustrated in Fig.-9(a). 98% degradation of 4-NA dye appeared at a concentration of 5 ppm.[25] As the concentration of dye increases, the number of dye molecules adsorbed on the surface of the catalyst increases and reduces the active sites available for catalytic reaction, which leads to a decrease in the rate of degradation.

Effect of Catalyst Dosage

The efficiency of the $SrSm_{0.09}Fe_{11.91}O_{19}$ catalyst at an optimal load was determined by varying the amount of catalyst from 5 to 20 mg per 100 mL and by adding 5 ppm of 4-NA dye. The highest percentage of degradation was attained for the 15 mg of the catalyst load, as shown in Fig.-9(b).[25] Hence, 15 mg of catalyst weight was chosen for the further photocatalytic experiments.

Effect of pH

The main parameter influencing the photocatalytic treatment of polluted water is pH. To obtain maximum degradation efficiency, the pH must be optimised. pH values varied from 2 to 12 to investigate the influence of pH on dye degradation, and the results are shown in Fig.-9 (c). The obtained results reveal that, at lower pH levels, the proportion of dye degradation was less. Therefore, the photocatalytic degradation increases with the pH, which may be due to to higher availability of •OH in alkaline medium and will create an additional $HO^{\cdot}$ Radical by interacting with holes produced by the catalyst's electronic excitation.[27,28]

Catalytic Recycling Studies

The photocatalytic stability was examined through the degradation process by a catalyst recycling process. The 40 mg catalyst and 10 ppm 4-nitro aniline (4-NA) were taken in a 100 mL solution and exposed to a sunlight source.[29] The degradation efficiency of $SrSm_{0.09}Fe_{11.91}O_{19}$ and the decomposition potency of 4-NA were the same for 3 cycles. Hence, this experiment showed that degradation efficiency greater than 52 % for the final cycle and the novel synthesized $SmSrFe_{12}O_{19}$ NP's stable even after five cycles.[30,31]

CONCLUSION

Samarium-doped strontium M-type hexagonal ferrites $SrFe_{12-x}Sm_xO_{19}$ (x=0, 0.01, 0.05, and 0.09) nanoparticles have been synthesized through the auto-combustion method. XRD investigation revealed the existence of a hexagonal structure with the absence of Sm_3O_3 as a separate phase. Scanning electron microscope platelets are like grains and have well well-defined hexagonal shape. FTIR analysis for pure and doped strontium ferrite samples shows that Fe-O stretching modes appear at around 587 $cm^{-1}$and also revealed that the introduction of Sm^{3+} ions could reduce the crystalline size. Hysteresis curves from VSM analysis indicate that at room temperature exhibited ferromagnetic behaviour for x=0.01 to 0.09. Coercivity more than 1.3kOe and investigated the hard magnetic nature of these samples. Results show that as the doping increases, Ms and Mr also increase continuously. Photo-degradation ability of $SrFe_{11.91}Sm_{0.09}O_{19}$ on Eriochrome black-T (EBT), methyl Orange (MO), methyl blue, and 4-nitroaniline(4-NA) dyes determined. All the dye degraded, but 985 degradation results were obtained for 4-nitroaniline. The energy band gap (Eg) is around 2.5 eV. Overall, the result indicated that the $SrSm_{0.09}Fe_{11.91}O_{19}$ was found to be an excellent photocatalyst for the dye degradation.

ACKNOWLEDGMENTS

We extended our thanks to USIC, University of Guwahati, Assam, for providing the VSM spectral data, and SAIF, Karnataka University, Dharwad, for providing TGA spectral data. And VGST-K-FIST(L1), Karnataka Government, Karnataka, India.

CONFLICT OF INTERESTS

The authors declare that there is no conflict of interest.

AUTHOR CONTRIBUTIONS

The present work is related to *SDG-12: Responsible Consumption and Production*. All the authors contributed significantly to this manuscript, participated in reviewing/editing and approved the final draft for publication. The research profile of the authors can be verified from their ORCID ids, given below:

A.Thippeswamy https://orcid.org/0009-0003-6238-9680

Prabhakar Chavan https://doi.org/0000-0001-8326-7154
G. Krishnamurthy https://orcid.org/0000-0002-5292-7858

REFERENCES

1. M.A. Hassaan, and M.A. El-Nemr, Elkatory, *Topics in Current,* **31,** 381(2023), https://doi.org/10.1007/s41061-023-00444-7
2. K. R. Sumadevi, G. Krishnamurthy, Prabhaker Walmik, R. S. Priya Rani, Satish Naik, H. S. Bhojya Naik and Nagaraja Naik, *Emergent Materials,* **4,** 447(2021), https://doi.org/10.1007/s42247-020-00153-7
3. M. A. Pugachevskii, D. S. Rasseko, V. A. Stupin, N. E. Manturova, E.B. Artyushkova and E. V. Silina, *Journal of Molecular Liquid,* **404,** 124946(2024), https://doi.org/10.1016/j.molliq.2024.124946
4. J. Lakshmikantha, G. Krishnamurthy, B. M. Nagabhushan, C. S. Naveen and E. Melagiriyappa, *Journal Superconductivity and Novel Magnetism,* **35,** 2485(2022), https://doi.org/10.1007/s10948-022-06223-7
5. C. Gao, Shi. J.W, Fan, Z.Y. Wang, B.R. Wang and Y.C He, *Applied Catalysis A*, **564**, 102(2018), https://doi.org/10.1016/j.apcata.2018.07.017
6. C. Yafet and Y. Kittle, *Physical Review Journal,* **87**, 290(2018), https://doi.org/10.1103/PhysRev.87.290
7. M. F. Lanjwani, M. Tuzen , M. Y. Khuhawar , T. A. Saleh, *Journal of Inorganic Chemistry Communication,* **159**, 111613(2024), https://doi.org/10.1016/j.inoche.2023.111613
8. K.R. Sumadevi, G. Krishnamurthy, H.S. Bhojya Naik, Prabhaker Walmik, Malathesh Pari, N. Ranjitha, R.S. Priya Rani, and P. Parameshwara Naik, *Asian Journal of Chemistry,* **33(10),** 2446(2021), https://doi.org/10.14233/ajchem.2021.23403
9. J. Lakshmikantha, G. Krishnamurthy, B. M. Nagabhushan, C. S. Naveen and E. Melagiriyappa, *Journal of Superconductivity and Novel Magnetism*, **35,** 2485(2022), http://dx.doi.org/10.1007/s10948-022-06223-7
10. J. W. Shi, J. T. Zheng, Y. Hu, Y. C. Zhao, *Journal of Environmental Engineering and Science,* **48** (2008), https://doi.org/10.1007/978-1-4471-5061-9-13
11. A. Thippeswamy, M.N. Manjunatha, Chavan Prabhakar, G. Krishnamurthy, *Analytical and Bioanalytical Electrochemistry*, **16(11)**,1026(2024), https://doi.org/10.22034/abec.2024.718628
12. J. Lakshmikantha, G. Krishnamurthy, R. Hanumantha Nayak, Malathesh Pari, N. Ranjitha, Nagaraj Naik, *Inorganic Chemistry Communication*, **146**, 110175(2022)
13. D. Srivastava and I. Lee, *Journal of Nanospheres*, **18,** 2471(2006), https://doi.org/10.1002/adma.200601123
14. N. Yasmin, M. Mirza, M. Safdar, M. Zahid, M. Ahmad, M.S. Awan and M. Altaf, *Journal of Magnetism and Magnetic Materials,* **17,** 31928(2017), http://dx.doi.org/10.1016/j.jmmm.2017.09.005
15. J. Lakshmikantha, G. Krishnamurthy, R. Hanumantha Nayak, Malathesh Pari, N. Ranjitha and Nagaraj Naik, *Inorganic Chemistry Communication*, **146**, 110175(2022),
16. N. K. Dung and N. T. L. Huyen, *Journal of Mathematical Physics,* **25**, 199(2009), https://doi.org/10.1016/j.matpr.2020.12.011
17. V. K Sankaranarayanan and D. C Khan, *Journal of Magnetism and Magnetic Materials,* **153,** 337(2020), https://doi.org/10.1016/j.matpr.2020.12.011
18. R. Skomski, U. Topal, Husnu Ozkan, and Huseyin Sozeri, *Journal of Magnetism and Magnetic Materials,* **284**, 416 (2004). https://doi.org/10.1016/j.jmmm.2004.07.009
19. R. C. Pulla, *Progress in Materials Science,* **57(7)**, 1191(2012), https://doi.org/10.1016/j.pmatsci.2012.04.001

20. X Liu, W. Zhong, S. Yang, Z. Yu and B.Y. Gu Du, *Journal of Magnetism and Magnetic Materials,* **238,** 207(2002), https://doi.org/10.1016/S0304-8853(01)00914-3
21. M. U. Ihsan Ali, M. S. Islam, M. Awan, Ahmad, M.N. Ashiq and S. Naseem, *Journal of Alloys and Compounds*, **550**, 564(2013), https://doi.org/10.1016/j.jallcom.2012.10.121
22. G. Joshi, A. Khot and S. Savant, *Journal of Materials Sciences: Materials in Electronics,* **65**, 159(2015), https://doi.org/10.1007/s10854-015-3031-2
23. K N. Harish, H. S. Bhojya Naik, P. N. Prashanth Kumar and R. Viswanath, *Catalysis Science and Technology,* **2,** 1033(2012), https://doi.org/10.1039/c2cy00503d
24. S. Gul, M.A. Yousuf, A. Anwar, M.F. Warsi, P.O. Agboola, I. Shakir and M. Shahid, *Ceramics International,* **46(9)**, 14195(2020), https://doi.org/10.1016/j.ceramint.2020.02.228
25. M. Anpo, G. Costentin, E. Giamello, H. Lauron-Pernot and Z. Sojka, *Journal of Catalysis,* **393** 259(2021), https://doi.org/10.1016/j.jcat.2020.10.011
26. H.C. Sathisha, Anitha, G. Krishnamurthy, Malathesh Pari, T.L. Soundarya and G. Nagaraju, *Chemical Data Collection,* **48** 10108(2023), https://doi.org/10.1016/j.cdc.2023.101081
27. G.V. Sree, P. Nagaraj, K. Kalanidhi, C.A. Aswathy and P. Rajasekaran, *Journal of Cleaner Production,* **270** 122294(2020), https://doi.org/10.1016/j.jclepro.2020.122294
28. H.S. Sumantha, S. Rajagopal, G. Nagaraju, M. Shashank and B.L. Suresha, *Chemical Physics Letters,* **779,** 138837(2021), https://doi.org/10.1016/j.cplett.2021.138837
29. D. Wang, M.A. Mueses, J. Angel, C. Marquez, F. Machuca-Martínez and I. Grcic, *Water Research.* **202**, 117421(2021), https://doi.org/10.1016/j.watres.2021.117421
30. M. Elansary, M. Belaiche, C. Ahmani Ferdi, E. Iffer and I. Bsoul, *RSC Advance*, **10,** 25239(2020), https://doi.org/10.1039/d0ra04722h
31. K.S. Jithendra Kumara, G. Krishnamurthy, N.S. Kumar, N. Naik, T.M. Praveen, *Journal of Magnetism and Magnetic Materials,* **451,** 8(2017), https://doi.org/10.1016/j.jmmm.2017.10.125

[RJC-9272/2025]